Triplet-exciton quenching in organic phosphorescent light-emitting diodes with Ir-based emitters

Sebastian Reineke, Karsten Walzer, and Karl Leo*
Institut für Angewandte Photophysik, Technische Universität Dresden, D-01062 Dresden, Germany
(Received 11 July 2006; revised manuscript received 31 January 2007; published 28 March 2007)

We investigate quenching processes which contribute to the roll-off in quantum efficiency of phosphorescent organic light-emitting diodes (OLED's) at high brightness: triplet-triplet annihilation, energy transfer to charged molecules (polarons), and dissociation of excitons into free charge carriers. The investigated OLED's comprise a host-guest system as emission layer within a state-of-the-art OLED structure—i.e., a five-layer device including doped transport and thin charge carrier and exciton blocking layers. In a red phosphorescent device, N,N'-di(naphthalen-2-yl)- N,N'-diphenyl-benzidine is used as matrix and tris(1-phenylisoquinoline) iridium [$Ir(piq)_3$] as emitter molecule. This structure is compared to a green phosphorescent OLED with a host-guest system comprising the matrix 4,4′,4″-tris (*N*-carbazolyl)-triphenylamine and the well-known triplet emitter *fac*-tris(2-phenylpyridine) iridium [$Ir(ppy)_3$]. The triplet-triplet annihilation is characterized by the rate constant k_{TT} which is determined by time-resolved photoluminescence experiments. To investigate triplet-polaron quenching, unipolar devices were prepared. A certain exciton density, created by continuous-wave illumination, is analyzed as a function of current density flowing through the device. This delivers the corresponding rate constant k_P. Field-induced quenching is not observed under typical OLED operation conditions. The experimental data are implemented in an analytical model taking in account both triplet-triplet annihilation and triplet-polaron quenching. It shows that both processes strongly influence the OLED performance. Compared to the red $Ir(piq)_3$ OLED, the green $Ir(ppy)_3$ device shows a stronger efficiency roll-off which is mainly due to a longer phosphorescent lifetime τ and a thinner exciton formation zone w.

DOI: 10.1103/PhysRevB.75.125328 PACS number(s): 73.40.Sx, 71.35.−y, 78.20.Bh, 78.47.+p

I. INTRODUCTION

The research interest in organic light-emitting diodes (OLED's) has grown tremendously in the last few years. In 1987, Tang and Van Slyke presented the first thin-film OLED utilizing two layers of organic material sandwiched between two electrodes in order to achieve light emission from one of the materials.[1] Tang *et al.* could enhance the efficiency by a factor of 2 by introducing a multilayer structure where the emission layer is doped with highly fluorescent materials.[2] The largest improvement of the external quantum efficiency of OLED's can be ascribed to the introduction of electrophosphorescent materials as a guest molecule of the emission layer (EML). In this case, the emission originates from radiative recombination of both singlet and triplet excitons, promising internal quantum efficiencies close to unity.[3–5] This corresponds to an external quantum efficiency (EQE, η_{ext}) of approximately 20%, which is limited by the outcoupling losses.[5,6] To further reduce the operating voltage and increase the quantum efficiency, the concept of doped transport layers for electrons and holes was introduced to electroluminescent devices,[7,8] leading to outstanding power efficiencies.[9]

Most possible applications like displays and large-area lighting demand OLED's to be operated at rather high brightness. While triplet emitters have improved the quantum efficiency, phosphorescent OLED's suffer from a decrease of efficiency when the current density is increased.[4,9] This is mainly due to the longer lifetime τ_{ph} of the emitting triplet state of organometallic complexes compared to the decay times of fluorescent dyes (τ_f in the range of nanoseconds).[10] Triplet-triplet annihilation, energy transfer to charged molecules (triplet-polaron quenching), and field-induced quenching are possible processes determining the quantum efficiency of phosphorescent OLED's and were analyzed previously.[11–15] Baldo *et al.* reported that triplet-triplet annihilation is the only dominating process determining the OLED quantum efficiency.[12]

Here, we demonstrate that both triplet-triplet annihilation (TTA) and triplet-polaron quenching (TPQ) can be observed under typical OLED operation conditions. Further we show that the dissociation of excitons or their precursor states due to the static electric field within the OLED is a very inefficient process in the discussed systems. Additionally, we investigated the recombination zone within the EML using a thin fluorescent layer to sense the phosphorescence. The width of this zone turns out to be an important parameter when it comes to the object of reduced EQE roll-off in phosphorescent OLED's. To model the experimental observations, a mathematical description of the OLED efficiency as a function of the current density is introduced, which combines TTA and TPQ. Using this model calculation, we demonstrate the different influence of each process and parameter on the OLED efficiency, respectively.

II. THEORETICAL DESCRIPTION

The theory necessary to describe various experiments in this study will be given here. All the investigated processes will be characterized by appropriate rate constants.

A. Triplet-triplet annihilation

For the first time, triplet-triplet annihilation has been reported by Kepler *et al.* where they observed delayed fluorescence in anthracene crystals.[16] Baldo *et al.* applied the con-

cepts given by Kepler *et al.* to the TTA processes observed in phosphorescent OLED's.[12] Their theoretical framework will be used as a basis in this work. The following assumptions are made: It is assumed that the excited singlet state of the emitting molecule ($^1M^*$) is quickly and efficiently transferred to the triplet state ($^3M^*$) via intersystem crossing (ISC) and, further, that only the guest molecules contribute to TTA. Adachi *et al.* showed a high rate of ISC for the phosphorescent emitter *fac*-tris (2-phenylpyridine) iridium, leading to a PL efficiency of nearly 100%.[4] Supporting those arguments, Tsuboi showed in his work that both a very weak singlet emission intensity and a very high ISC rate of 98.7% can be observed for $Ir(ppy)_3$ at 10 K.[17] Even at room temperature, the singlet emission intensity can be neglected. Further, those assumptions are only valid when the host-guest energy transfer is highly efficient and, therefore, close to unity. In this case, the host emission is completely quenched by the emitter dopant. The energy of a donor molecule can be exchanged via Förster-type energy transfer to an excited acceptor molecule.[18,19] Dexter-type transfer is also possible; nevertheless, this requires orbital overlap and, therefore, a short interaction distance.[20] Finally, the TTA can be expressed by one reaction

$$^3D^* + {}^3A^* \overset{k_{TT}}{\rightarrow} {}^1D + {}^3A^*, \tag{1}$$

where D and A represent the corresponding donor and acceptor molecules, respectively. After the annihilation process, the excited acceptor molecule $^3A^*$ is still contributing to the overall triplet exciton density which is indicated by the 1/2 in the following equation. Under a short-pulse optical excitation, the time development of the triplet exciton population can be written as

$$\frac{d[n_{ex}]}{dt} = -\frac{[n_{ex}]}{\tau} - \frac{1}{2}k_{TT}[n_{ex}]^2, \tag{2}$$

which can be solved to

$$L(t) = \frac{L(0)}{\{1 + [n_{ex}(0)]k_{TT}\tau/2\}e^{t/\tau} - [n_{ex}(0)]k_{TT}\tau/2}. \tag{3}$$

Here, it is assumed that the luminescent intensity L is linearly proportional to the concentration of excited states ($L(t) \sim [n_{ex}(t)]/\tau$).[12] Further, k_{TT} is the rate constant for TTA and τ, unless otherwise specified, the phosphorescent lifetime.

B. Triplet-polaron quenching

Early reports on interactions between triplet excitons and trapped charges were made by Ern *et al.* in anthracene crystals.[21] They introduced a rate equation to describe this bimolecular process. In order to investigate TPQ, experiments were carried out involving continuous-wave (cw) illumination and steady-state current flow. They will be explained in detail in the following section. Depending on the type of charge, the quenching process can occur as

$$^3D^* + A^+ \overset{k_{P,h}}{\rightarrow} {}^1D + A^{+,*}, \tag{4}$$

$$^3D^* + A^- \overset{k_{P,e}}{\rightarrow} {}^1D + A^{-,*}. \tag{5}$$

Again, this process is mainly a Förster-type transfer where no direct orbital overlap is necessary.[19] Assuming that the rate of triplet-polaron quenching is proportional to the charge-carrier density $[n_c] \equiv [n_c](j) = [\rho_c(j)/e]$, the differential equation reads[12,21]

$$\frac{d[n_{ex}]}{dt} = -\frac{[n_{ex}]}{\tau} - k_P\left[\frac{\rho_c(j)}{e}\right][n_{ex}] + G, \tag{6}$$

where k_P is the TPQ rate constant, e the elementary charge, and G a constant term describing the cw illumination. According to space-charge-limited current (SCLC) theory,[22] further assuming that

$$V \simeq \frac{\rho_c}{\varepsilon_r\varepsilon_0}d^2, \tag{7}$$

with charge density ρ_c, voltage V, and thickness of the EML, d,[23] the rate equation can be transformed to the following expression:

$$\frac{d[n_{ex}]}{dt} = -\frac{[n_{ex}]}{\tau} - k_P C j^{1/(l+1)}[n_{ex}] + G, \tag{8}$$

$$C := \left[\left(\frac{l+1}{2l+1}\right)\left(\frac{l+1}{l}\right)^l\left(\frac{N_t^l\varepsilon}{de^2\mu N_c}\right)\right]^{1/(l+1)}, \tag{9}$$

where N_c is the density of states at the transport level, N_t the density of trap states, and $l = E_t/kT$ (E_t, depth of trap states). Additional trap states are implemented to be able to describe the most general case. As the data analysis will show later, the use of the simple Mott-Gurney relation ($l=1$) reveals the best agreement. The case of field-dependent mobility, as is often reported in literature,[24] cannot be applied here in order to obtain an analytical solution. The steady-state condition of Eq. (8) can be solved to an equation which can be used to analyze the data of the above named experiments:

$$\frac{\eta_{TP}(j)}{\eta_0} = \frac{1}{(1 + \tau k_P C j^{1/(l+1)})}. \tag{10}$$

The parameter C is describing microscopic properties of a certain system—e.g., the mobility, dielectric constant—which can only be estimated. For analysis, this parameter is kept constant while k_P is used to fit the data. Therefore, k_P reflects different transport properties of electrons and holes of a specific system as well.

C. Unified model

Both triplet-triplet annihilation and triplet-polaron quenching will now be combined in one rate equation, which reads

$$\frac{d[n_{ex}]}{dt} = -\frac{[n_{ex}]}{\tau} - \frac{1}{2}k_{TT}[n_{ex}]^2 - k_P\left[\frac{\rho_c(j)}{e}\right][n_{ex}] + \frac{j}{ew}. \tag{11}$$

According to Baldo *et al.*, j/ew is introduced to describe the exciton generation under electroluminescent (EL)

conditions.[12] Here, w is the thickness of the exciton formation zone. The steady-state solution ($d[n_{ex}]/dt=0$) of this equation needs to be deduced to describe the typical OLED operation. Using the same relationships for the charge-carrier density n_c as previously shown, the solution reads

$$\frac{\eta(j)}{\eta_0} = \Theta\left[\sqrt{\frac{\Delta^2+\Gamma k_{TT}}{k_{TT}^2}} - \frac{\Delta}{k_{TT}}\right], \tag{12}$$

with

$$\Theta = \frac{ew}{\tau j}, \tag{13}$$

$$\Delta \equiv \Delta(k_P) = \left(\frac{1}{\tau} + k_P C j^{1/(l+1)}\right), \tag{14}$$

$$\Gamma = \frac{2j}{ew}. \tag{15}$$

Equation (12) can be used to fit the external quantum efficiency of phosphorescent OLED's. It can be seen that the behavior is determined by four parameters τ, k_{TT}, k_P, and w. In this study, all parameters are determined in experiments, allowing us to directly test this model.

III. EXPERIMENT

All devices and layers of interest are prepared by thermal evaporation on precleaned substrates. Depending on the application, quartz glass or regular glass substrates are used. In the case of OLED's and unipolar devices, the glass substrates are coated with patterned indium tin oxide (ITO) bottom contacts ($\sim$25 Ω/sq, $d=132$ nm). The evaporation of organic materials is performed under high-vacuum (HV) conditions ($\sim 10^{-7}$ mbar). The top contact is evaporated under HV as well without the need to break the vacuum during device preparation. All samples are encapsulated in a nitrogen atmosphere to avoid contamination by the ambient.

A. Phosphorescent OLED's

Two phosphorescent OLED's are investigated in this study. They basically differ in their emission layer. This EML is within a five-layer OLED architecture. Hole (HTL) and electron (ETL) transport layers are p- and n-doped, respectively. All materials are purchased from commercial distributors as stated subsequently. Every organic material is purified by high-vacuum gradient sublimation. For the HTL, N,N,N'',N'-tetrakis(4-methoxyphenyl)-benzidine (MeO-TPD, Sensient) is doped with 2,3,5,6-tetrafluoro-7,7,8,8-tetracyano-quinodimethane (F_4-TCNQ, TCI Europe).[7] The electron transport layer comprises Cs-doped 4,7-diphenyl-1,10-phenanthroline (BPhen, Fluka).[25] Adjacent to those transport layers, thin intrinsic electron (EBL) and hole (HBL) blocking layers are deposited. As EBL and HBL, N,N'-di(naphthalen-2-yl)-N,N'-diphenyl-benzidine (NPB, Sensient) and BPhen are used, respectively. The Cs dispenser is purchased from SAES Getters S.p.A., Italy.

The EML of the red OLED comprises a host-guest system of NPB and tris(1-phenylisoquinoline) iridium [$Ir(piq)_3$, American Dye Source], where $Ir(piq)_3$ is the phosphorescent emitter molecule with a doping concentration of 20 wt %. In contrast to this diode, the green OLED comprises 4,4′,4″-tris (N-carbazolyl)-triphenylamine (TCTA, Sensient) as matrix and *fac*-tris(2-phenylpyridine) iridium [$Ir(ppy)_3$, American Dye Source] as triplet emitter.[9] Here, $Ir(ppy)_3$ is doped into TCTA with 7 wt %. The corresponding OLED structure is depicted in Fig. 1. The evaluation of the OLED's presented in this study is done according to a standard procedure reported elsewhere.[9]

B. Unipolar devices

To study triplet-polaron quenching, it is necessary to investigate the influence of charge carriers on triplet excitons. Therefore, charge carriers and excitons need to be created separately. Unipolar devices have a modified architecture compared to OLED structures. Due to the suitable choice of energy levels, the transport of only one charge type, either electrons or holes, can be achieved. An energy level diagram of such a device can be seen in Fig. 1. The remaining layers are kept as close to the OLED structure as possible. Doped transport layers are important to assure that the main contribution to SCLC is within the comparably thin intrinsic layers. This is necessary to estimate the charge carrier density later on. The blocking layers adjacent to the EML are inserted to avoid exciton quenching at the interfaces to the doped transport layers.

C. Time-resolved measurements

Time-resolved PL experiments are carried out to investigate triplet-triplet annihilation. Therefore, a thin film of the OLED emission layer is deposited on quartz glass. To avoid contamination by the ambient, this sample is afterwards encapsulated with another quartz glass under nitrogen atmosphere. The samples are excited with a pulsed TEM_{00} nitrogen laser MSG-SD from Lasertechnik Berlin GmbH, having a wavelength of 337 nm and a pulse length of approximately 500 ps. The PL signal from the excited sample is collected with a set of two lenses to a fast PDA 55 photodiode (Thorlabs GmbH, Karlsfeld). The signal is recorded in a fast multichannel oscilloscope (Infinium 54815A from Hewlett-Packard, Houston). A powermeter with a suitable detector head 318J09B (Newport GmbH, Darmstadt) is used to determine the energy of the laser pulse. An iris diaphragm is placed in direct proximity of the sample within the laser-sample path to cut the low-intensity range of the Gaussian TEM_{00} distribution. Different neutral filters are used to attenuate the pulse intensity. For the investigation of EL transients, a pulse generator (8114A from Hewlett Packard, Houston) is used to excite the OLED in a pulsed mode.

D. Steady-state PL experiments

As mentioned above, unipolar devices can be used to obtain controlled injection of one type of carriers to the EML of interest. To investigate the interaction between charges (po-

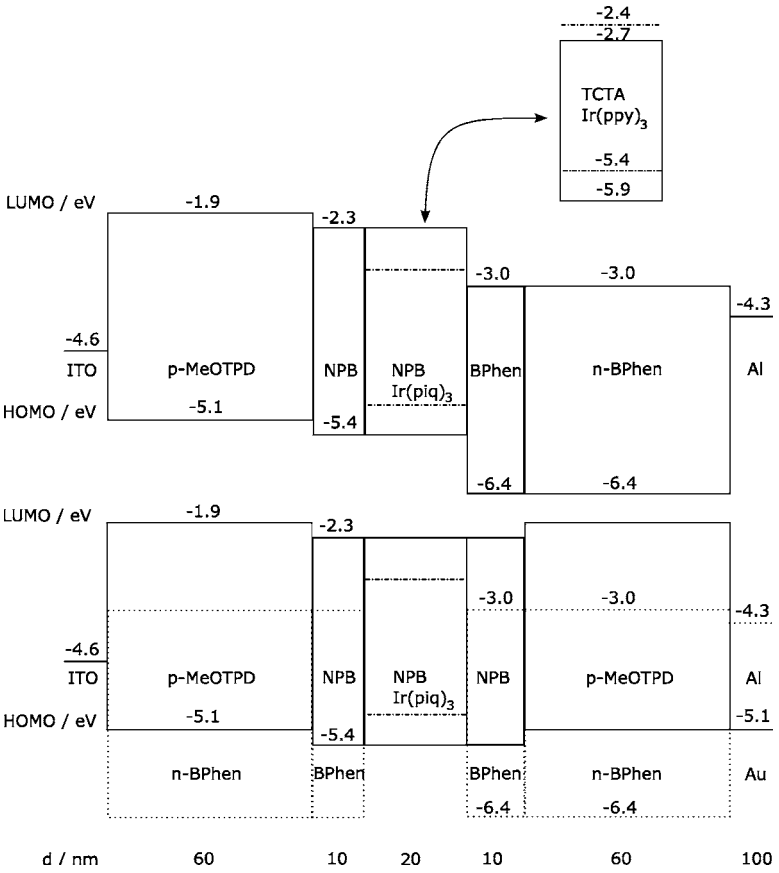

FIG. 1. Proposed energy level diagram of the red OLED (top) and corresponding unipolar devices (bottom) used in this study comprising $Ir(piq)_3$ as phosphorescent emitter molecule. The HOMO and LUMO values for $Ir(piq)_3$ are not known. The same structures were used for the green OLED with an EML of TCTA:$Ir(ppy)_3$. Bottom: unipolar devices (hole only, solid lines; electron only, dotted lines).

larons) and excitons, the latter are created separately by illuminating the sample with a IK5351R HeCd laser (Kimmon Electric Co., Tokio). The laser wavelength (325 nm or 442 nm) is chosen to fit the spectral range of strong matrix absorption as well as possible. The current density flowing through the sample is controlled by a source measure unit SMU 2400 from Keithley Instruments, Inc., Cleveland. The PL spectrum of the unipolar device is detected by a FluoroMax spectrometer (Horiba Jobin Yvon GmbH, Munich) as a function of current density j. The current density is varied from 0.1 to 200 mA/cm^2, which is a typical range for OLED operation.

E. Fluorescent sensitizer

The technique of thin sensing layers is applied to the EML of the OLED's discussed here.[26] Therefore, a blue fluorescent material, 2,2′,7,7′-tetrakis(2,2-diphenylvinyl)spiro-9,9′-bifluorene (Spiro-DPVBi, Merck), is deposited at different positions within the EML. Here, the sensing is accomplished by triplet exciton quenching—i.e., the triplet level of the fluorescent material is lower than the triplet level of the phosphor (see Fig. 2). Under such conditions, the triplet exciton formed on the phosphorescent molecule can be transferred to the nonradiative triplet level of the fluorescent material. Those excitons cannot contribute to the emission anymore. Mainly two conditions need to be fulfilled to extract information about the recombination behavior within the EML. Those are that (i) the additional layer should not affect the transport properties of the device and (ii) the quenching should be a locally confined process. To avoid energy barriers (i), the layer is kept to an effective thickness of 1 nm which does not form a closed layer. The triplet energy transfer is a Dexter-type transfer which requires notice-

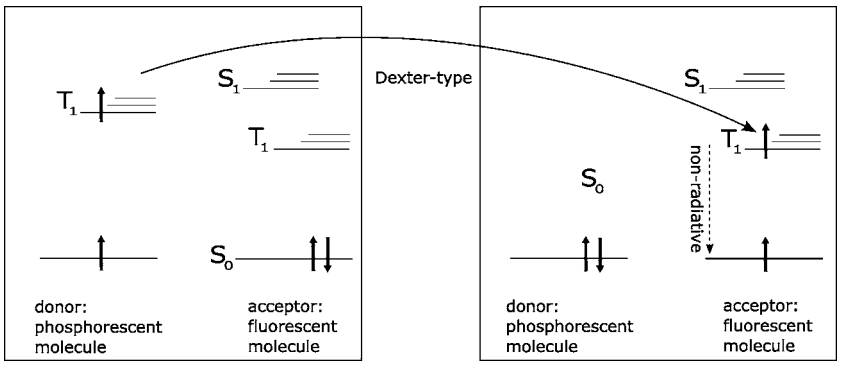

FIG. 2. Scheme of the exciton energy transfer from a phosphorescent donor molecule to a fluorescent acceptor molecule. Here, the singlet state of the fluorescent sensitizer is higher and the nonradiative triplet level is lower or equal to the triplet state of the donor, respectively.

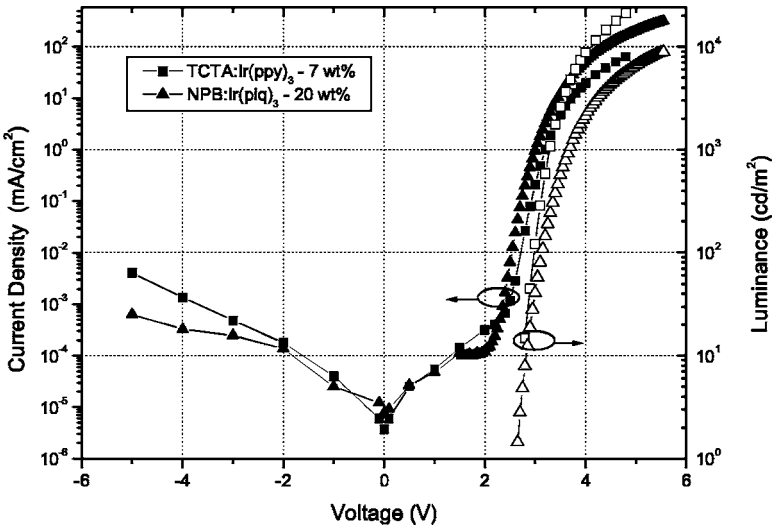

FIG. 3. *j-V* characteristics and corresponding luminance data of the two OLED structures presented here. They differ only in the choice of the EML.

able orbital overlap of donor and acceptor molecule. It can be expressed as follows:

$$^3D^* + {}^1A \rightarrow {}^1D + {}^3A^*. \quad (16)$$

This transition is strictly forbidden in terms of the Förster mechanism since it would require two simultaneous intersystem crossing steps. The typical interaction distance of this transfer is up to 1 nm, assuring condition (ii).[20]

IV. RESULTS

In order to discuss the investigated quenching processes, two phosphorescent OLED's are selected to serve as examples in this study. The OLED's only differ in the EML which are comprising a host-guest system of TCTA:$Ir(ppy)_3$ and NPB:$Ir(piq)_3$, respectively. The *j-V* characteristics as well as the electroluminescent intensity versus voltage are shown in Fig. 3. The corresponding external quantum efficiencies of those OLED's will be shown and discussed in detail in the following sections. The corresponding absorbance and luminescent data of those systems are depicted in Fig. 4.

A. Triplet-triplet annihilation

Triplet-triplet annihilation is investigated by analyzing the PL transients. For this, a mixed film of either TCTA:$Ir(ppy)_3$ or NPB:$Ir(piq)_3$ is excited by a short laser pulse. The samples are deposited on and encapsulated with quartz glass to avoid glass fluorescence and oxygen quenching, respectively. The excitation intensity and, therefore, the exciton density within the sample are varied over three orders of magnitude. The time decay of both EML systems can be seen in Figs. 5 and 6. To achieve a good signal-to-noise ratio, those decay curves represent the average of approximately 500 detection cycles.

It can be seen that there is an initial faster decay. This effect increases with increasing excitation intensity. Then, all transients result in an exponential decay behavior which indicates monomolecular decay. The strong initial decay can be attributed to a bimolecular quenching effect—i.e., triplet-

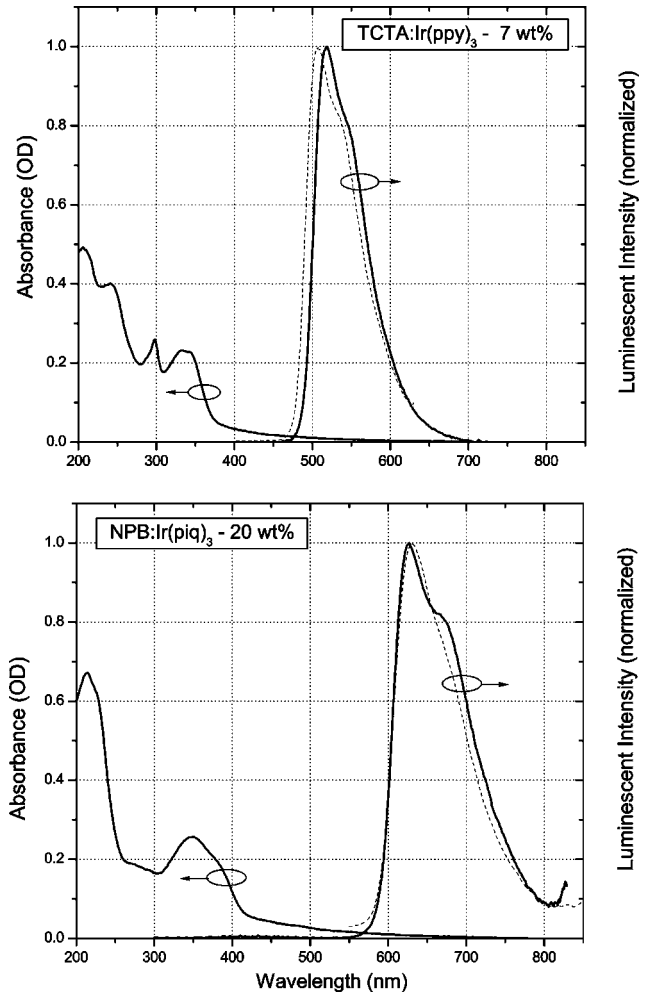

FIG. 4. Absorbance (OD=optical density) and luminescent intensity of the mixed layer used as EML in this study. The solid and dashed lines represent EL and PL, respectively. The thickness of the layers is 20 nm. Neither of both systems shows a contribution of matrix emission in the EL spectrum, indicating very efficient host-guest energy transfer.

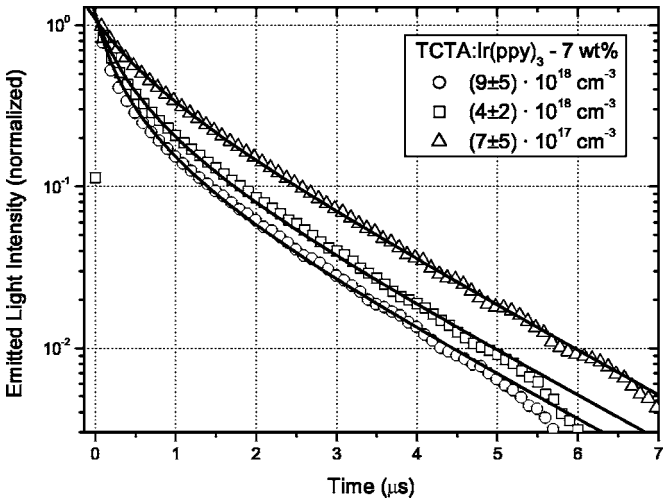

FIG. 5. Time decay of a TCTA:$Ir(ppy)_3$ PL sample at different excitation intensities indicated by the determined initial exciton density. Solid lines indicate calculations according to Eq. (3).

triplet annihilation. Using Eq. (3) and knowing the initial exciton density $[n_{ex}]$, the TTA rate constant can be derived. As mentioned in Sec. III C, an iris diaphragm is used to cut the laser intensity directly before the sample. In a reference measurement, the intensities of the laser with and without iris diaphragm (diameter 3 mm) are (1.1 ± 0.1) μJ and (0.2 ± 0.1) μJ, respectively. Assuming a Gaussian intensity distribution of the laser beam, one can estimate that the energy of the exciting spot varies from maximum to appoximately $(96\pm1)\%$ at the outer edge of the spot. Therefore, to estimate the exciton density $[n_{ex}]$ within the sample, it is assumed that the excitation intensity of the spot is constant in directions normal to the light propagation. The solid lines in Figs. 5 and 6 represent the corresponding calculated fit. There, the curves are normalized for better comparison. Furthermore, the radiative lifetime τ can be determined. All parameters which were used and derived from this experiment are summarized in Table I. The motivation for the mean value of k_{TT} and τ will be given later. One can find the main

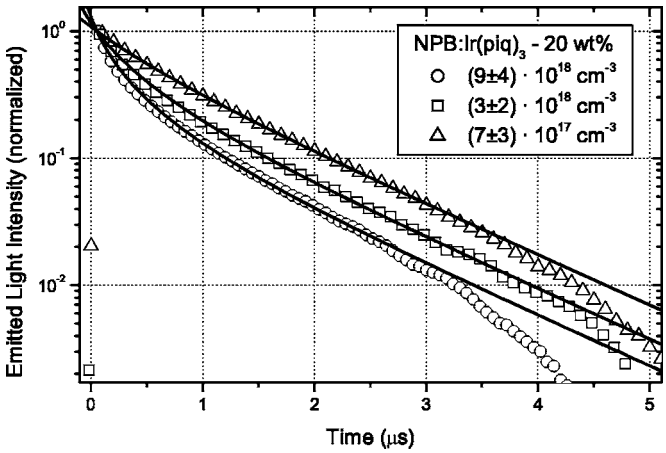

FIG. 6. Time decay of a NPB:$Ir(piq)_3$ PL sample at different initial exciton densities (cf. Table I). Solid lines represent calculations according to Eq. (3).

TABLE I. Summary of parameters determined in the time-resolved PL experiments.

	$[n_{ex}]$ $[\mathrm{cm}^{-3}]$	k_{TT} $[10^{-12}\ \mathrm{cm}^3\ \mathrm{s}^{-1}]$	τ $[\mu s]$
TCTA:$Ir(ppy)_3$			
	$(9\pm5)\times10^{18}$	(0.8 ± 0.4)	(1.60 ± 0.05)
	$(4\pm2)\times10^{18}$	(1.0 ± 0.6)	(1.60 ± 0.05)
	$(7\pm5)\times10^{17}$	(2 ± 1)	(1.58 ± 0.05)
	$(3\pm2)\times10^{17}$	(3 ± 2)	(1.58 ± 0.05)
	$(9\pm5)\times10^{16}$	(7 ± 4)	(1.56 ± 0.05)
	Mean value	**(3±2)**	**(1.58±0.05)**
NPB:$Ir(piq)_3$			
	$(9\pm4)\times10^{18}$	(0.8 ± 0.4)	(1.10 ± 0.05)
	$(3\pm2)\times10^{18}$	(1.0 ± 0.5)	(1.10 ± 0.05)
	$(7\pm3)\times10^{17}$	(2 ± 1)	(1.10 ± 0.05)
	$(3\pm1)\times10^{17}$	(2 ± 1)	(1.10 ± 0.05)
	$(8\pm3)\times10^{16}$	(1.0 ± 0.5)	(1.10 ± 0.05)
	Mean value	**(1.4±0.6)**	**(1.10±0.05)**

difference between the two EML systems in the radiative lifetime and triplet-triplet annihilation rate constant. For TCTA:$Ir(ppy)_3$, the lifetime τ is about 1.5 times greater than for NPB:$Ir(piq)_3$. Within the experimental error, the triplet lifetime can be seen as constant in the range of excitation intensity applied here. The rate constant k_{TT} is slightly smaller in the NPB:$Ir(piq)_3$ case. The error of the TTA rate constant is rather high which makes interpretation difficult. This partly stems from the determination of the exciton density which is influenced by several sources of error. Here, mainly the determination of the thickness d of the sample, which is controlled by quartz crystal monitors ($\Delta d/d \sim 0.5\%$), and the spot size (diameter d_s) of the exciting laser beam contribute to the systematic error. The latter, even though the iris diaphragm is placed in direct proximity of the sample, is influenced by a fairly strong divergence of the laser beam, resulting in ($\Delta d_s/d_s \sim 1.5\%$). Nevertheless, the experiment reveals the order of magnitude of this bimolecular quenching process. Kalinowski *et al.* estimated the TTA rate constant to a value of $k_{TT}=(1-3)\times10^{-12}$ $\mathrm{cm}^3\ \mathrm{s}^{-1}$ for a mixed layer of bisphenol-A-polycarbonate and N,N'-diphenyl-N,N'-bis(3-methylphenyl)-(1,1′-biphenyl)-4,4′-diamine (PC and TPD) doped with 6% of $Ir(ppy)_3$ which nicely agrees with our results.[27] Both Holzer *et al.* and Baldo *et al.* reported about TTA in a system of approximately 8 wt % of $Ir(ppy)_3$ dispersed in a 4,4′-N,N'-dicarbazole-biphenyl (CBP) matrix.[11,28] In the latter work, neither the EL transients nor the steady-state EQE versus current density behavior could be fitted with a single value of k_{TT} and τ. Without having a detailed explanation for those results, they appoint their finding to triplet-host interactions. Holzer *et al.* reported $k_{TT}=1.6\times10^{-10}$ $\mathrm{cm}^3\ \mathrm{s}^{-1}$ and $k_{TT}=8.8\times10^{-11}$ $\mathrm{cm}^3\ \mathrm{s}^{-1}$ for estimated initial exciton densities of 3.2×10^{17} cm^{-3} and 3.2×10^{18} cm^{-3}, respectively. If one compares the latter data pair with values of this work corresponding to equal initial exciton densities, Holzer *et al.* ob-

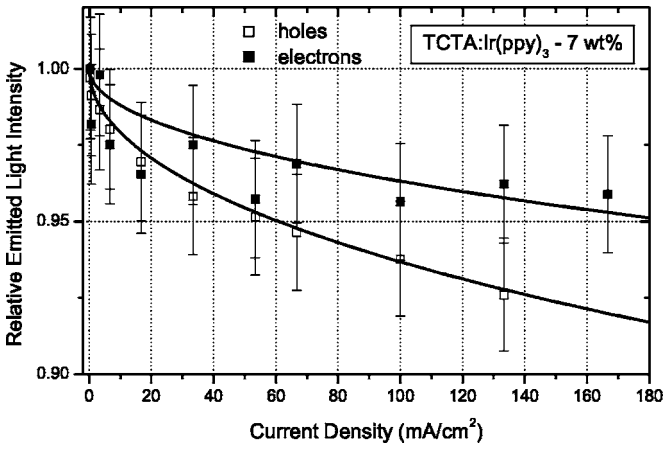

FIG. 7. PL intensity of unipolar devices comprising TCTA:$Ir(ppy)_3$ as EML. Solid lines represent the fit calculation according to Eq. (10).

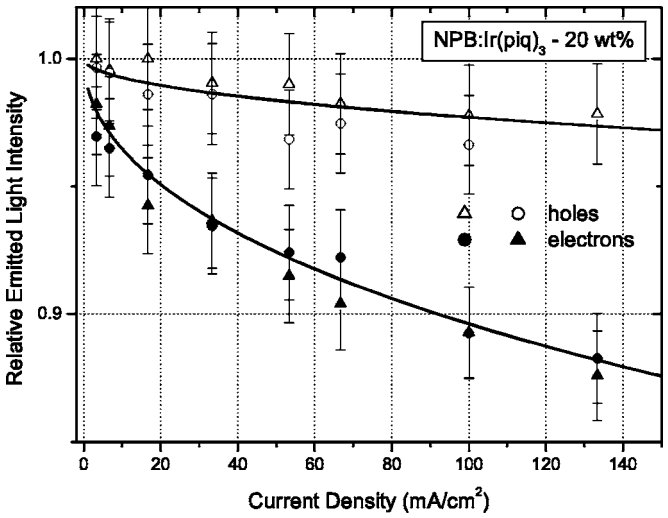

FIG. 8. PL intensity of unipolar devices comprising NPB:$Ir(piq)_3$ as EML. Solid lines represent the fit calculation according to Eq. (10). This plot shows two independent sets of data, revealing the reliability of the experiment.

served a k_{TT} which is about two orders of magnitude higher. In contrast to the samples in this work, Holzer *et al.* prepared their samples by spin coating, a method with strong difference to thermal evaporation. Using the data at hand, a higher degree of aggregation during the spin-coating process could be the origin of this increased TTA.

B. Triplet-polaron quenching

To study the quenching process between charge carriers and triplet excitons—i.e., the triplet energy transfer to charged molecules—the PL of unipolar devices is investigated. The structure of the corresponding device structures can be seen in Fig. 1. Depending on the type of charge (electron or hole), either aluminum (Al) or gold (Au) is used to assure Ohmic contacts to the adjacent transport layers. The PL intensity decreases with increasing current density j flowing through the samples. The relative intensity is plotted in Figs. 7 and 8. For both EML systems there are two sets of data which correspond to a hole- and electron-only current, respectively.

Equation (10) can be used to fit the data displayed in Figs. 7 and 8. It is obvious that the value C in this equation depends on the transport properties of a certain material complex—i.e., the charge carrier mobility μ. Unfortunately, this material property is not known for each material system and charge. To investigate the experimental data, the mobility is set to a certain value of $\mu=1\times10^{-6}$ cm^2 $(V\ s)^{-1}$ and kept fixed for all fit calculations. For molecular organic semiconductors, as they are used in this study, this is a typical mobility value.[29] Therefore, the fit parameter k_P in Eq. (10) holds information about the transport properties of the system as well. The triplet lifetime τ was used as determined from previously discussed time-resolved experiments (see Table I). Furthermore, the value C depends on N_c, the density of states at the transport level, N_t, the density of trap states, and ε_r, the relative permittivity. In this calculation, N_c and N_t were determined by the density of matrix and dopant molecules, respectively, and the relative permittivity was set to a value of $\varepsilon_r=3.5$.[29] As mentioned in Sec. II, Eq. (10) is based on SCLC theory. A great advantage in this study is the use of doped transport layers. Therefore, one can assume that space charge is found only within the intrinsic layers—i.e., the EML and the thin blocking layers. Here, the influence of the blocking layers is neglected since they favor the transport of the corresponding charges (either holes or electrons). The best fits are achieved using a value $l=1$ for the parameter $l=E_t/kT$. This is the special case of SCLC where trap states do not influence the transport—i.e., the Mott-Gurney case.[22] In contrast to this dependence, the unipolar devices reveal a value of $l=(2.0\pm0.4)$ throughout our study.[29] The difference between the latter and the results from the data fit can have various origins—e.g., energy barriers which give a small contribution of injection limitation to the current. One could also think that there is a difference between the real charge carrier density within the device and an effective charge carrier density contributing to the TPQ. The only conclusion one can make at this point is the following. The triplet-polaron quenching shows a current dependence as if the charge carrier density would increase according to the Mott-Gurney relation. The various values of the triplet-polaron rate constant k_P are summarized in Table II. This experiment shows that TPQ is clearly observed in the range of current densities j typical for OLED operation. This supports the intention of this study to include of TPQ in model calculations of OLED quantum efficiency. One can see that $k_P \equiv k_{P,e}$ is greater in the NPB:$Ir(piq)_3$ device for electron cur-

TABLE II. Triplet-polaron rate constants derived from fit calculations according to Eq. (10). Indices represent the type of charge, electron, or hole, respectively.

	$l=E_t/kT$	$k_{P,e}$ $[10^{-12}\ cm^3\ s^{-1}]$	$k_{P,h}$ $[10^{-12}\ cm^3\ s^{-1}]$
TCTA:$Ir(ppy)_3$	1	(0.2 ± 0.1)	(0.3 ± 0.2)
NPB:$Ir(piq)_3$	1	(0.7 ± 0.2)	(0.2 ± 0.1)

rents. This, again, is a superposition of microscopic quenching cross section and transport property. Therefore, it cannot be distinguished whether the cross section is larger in this case or not. Nevertheless, for that specific EML system and charge, the effective quenching due to charges is more pronounced. Baldo and Forrest reported triplet-polaron quenching with a corresponding rate constant of $k_P = 1 \times 10^{-12}\ \mathrm{cm}^3\ \mathrm{s}^{-1}$ in an unipolar electron transport device comprising an emitting system of aluminum tris (8-hydroxyquinoline) (Alq_3) and 2,3,7,8,12,13,17,18-octaethylporphine platinum (PtOEP).[30] Kalinowski *et al.* reported $k_P = (5.0-7.5) \times 10^{-12}\ \mathrm{cm}^3\ \mathrm{s}^{-1}$ for a PC:TPD:$Ir(ppy)_3$-emitting system within an OLED structure.[14] Compared with those results, the triplet-polaron quenching rate constants in this work are slightly smaller for both electron and hole currents. But as mentioned above, this value can shift to the one or other direction taking into account the missing information about the actual transport properties.

C. Field-induced triplet exciton quenching

Excitons, or their precursor states prior to the exciton formation, can also be quenched by dissociation into free charges due to an applied electric field.[14] This has been reported by various research groups for both singlet and triplet excitons.[13,14,31] First of all, the effective field present in the OLEDs needs to be estimated. Due to the use of doped transport layers in this study, the effective field within the device can be calulated as follows:

$$F = \frac{U}{d_{in}} - \frac{U_{bi}}{d_{in}}, \tag{17}$$

where U_{bi} is the built-in potential and d_{in} the thickness of the intrinsic (nondoped) layers. The built-in potential is roughly determined by the difference between the lowest unoccupied molecular orbital (LUMO) level of the *n*-doped ETL and the highest occupied (MO) (HOMO) of the *p*-doped HTL. This results in $U_{bi} \sim 2$ V. Referring to Fig. 3, one can estimate the upper limit of applied field strength to $F \sim 0.75$ MV/cm at 5 V operating voltage. Now there are two possible processes which can quench the luminescence: the (i) amplitude quenching and (ii) rate quenching mechanisms.[31] One can distinguish between both processes in time-resolved measurements. In the case of amplitude quenching (i), the electric field dissociates a precursor to the emitting state which leads to a decrease of the initial PL amplitude. Different from the latter, the rate quenching mechanism (ii) is determined by quenching of the final emissive state, resulting in a shorter lifetime. Two experiments were carried out to investigate the process of field-assisted quenching, one under photo excitation, the other under electrical excitation.

The PL transients were recorded as a function of the applied electric field. Therefore, an OLED structure was excited as described in Sec. III C. Additionally, the applied field was increased in backward bias direction from a roughly field-free condition up to 2.5 MV/cm. Applying backward bias to an OLED has the great advantage in investigating the influence of the electric field while the current density *j* is very low. The result can be seen exemplarily for

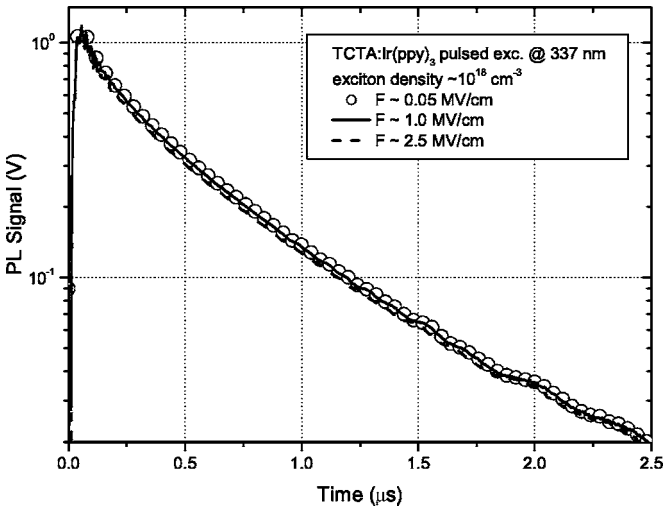

FIG. 9. PL time decay of the TCTA:$Ir(ppy)_3$ based OLED with variation of the effective electric field strength *F*. The sample is excited with a laser pulse as described in the previous sections.

the TCTA:$Ir(ppy)_3$ device in Fig. 9. No difference, either in amplitude or in lifetime, can be observed up to a field of 1.0 MV/cm. A small amplitude decrease of 5% can be seen at a field strength of approximately 2.5 MV/cm. This value exceeds the upper limit of OLED operation conditions at least by a factor of 2. The NPB:$Ir(piq)_3$ system revealed the same experimental findings.

In a second experiment, the OLED's were pumped with a short voltage pulse with an amplitude of 6.6 V and a duration of 20 μs. The EL mode assures that the exciton dynamics including their generation can be investigated as it is present within an OLED. Directly after the positive voltage pulse, the voltage is switched to negative values, resulting in an electric field during the exciton decay. The EL transients and the corresponding effective field strength *F* can be seen in Fig. 10 for NPB:$Ir(piq)_3$. One can see that the EL decay is unaffected by the field variation. The oscillation visible shortly after the positive voltage pulse is most likely due to the OLED capacitance. This also explains the increasing field strength in the first few microseconds. Once again, this result coincides with the data of the structure comprising $Ir(ppy)_3$ as emitter molecule which is, therefore, not shown. In conclusion and different from previous works—e.g., by Kalinowski *et al.*[14]—field-assisted exciton quenching can be ruled out as the reason for the EQE roll-off in state-of-the-art phosphorescent OLED's. This is reasonable considering the localized nature of the excited triplet state. One can roughly estimate the energy which is necessary to dissociate a triplet state by comparing the HOMO-LUMO gap and the triplet state energy. For the case of $Ir(ppy)_3$, the triplet energy is (2.4±0.1) eV,[11] while the HOMO-LUMO gap is 3.0 eV.[9] This results in an exciton binding energy of approximately 0.6 eV which is supporting the experimental data that field-induced exciton dissociation is unlikely under OLED operation conditions.Those results make it reasonable to exclude a second order term in Eq. (11) (cf. Sec. II C) describing field-induced quenching.

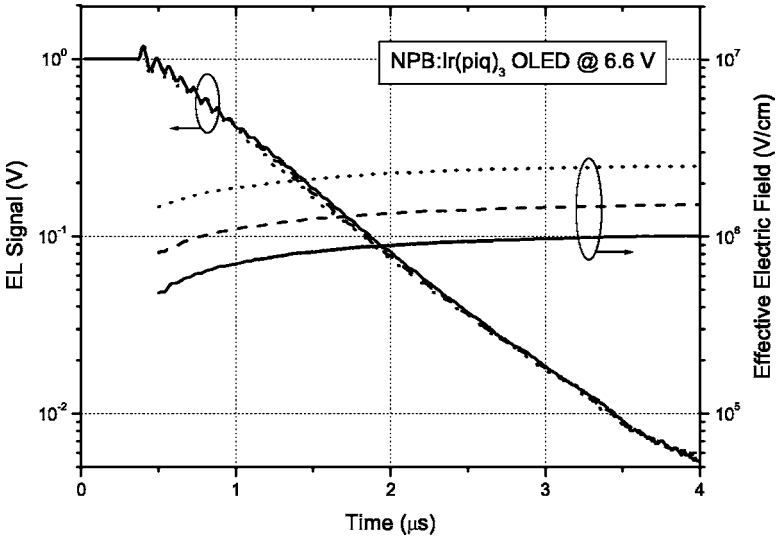

FIG. 10. EL time decay of the NPB:$Ir(piq)_3$ based device. Here, a 20-μs positive voltage pulse is used to pump the OLED. The plotted field strength F is achieved by applying a negative voltage immediately after the EL pump pulse.

D. Exciton recombination zone

In Fig. 11, the j-V characteristics of OLED structures with and without additional sensing layer are shown. One can see that the presence of such layers does not affect the transport properties of the OLED. Therefore, it can be assumed that the exciton generation is not affected as well.

For both OLED's, the electroluminescent intensity relative to the respective standard OLED is plotted as a function of the position of the sensing layer in Fig. 12. These data are collected for different current densities. Of course, the two EML's differ in the emitter molecule. Therefore, the efficiency of energy transfer to the nonradiative triplet state of Spiro-DPVBi is different. It is reasonable to assume that the energy transfer from $Ir(ppy)_3$ to Spiro-DPVBi is an exothermic process due to a high triplet energy of the phosphor. On the other hand it is not clear whether the energy transfer in the case of $Ir(piq)_3$ is still exothermic. One could imagine that the lower triplet energy of the red emitter results in endothermic energy transfer. Nevertheless, it is shown in Fig. 12 that quenching is observed in both cases. The fact that the relative luminance does not return to a value of unity can be explained by minor contributions of exciton diffusion.

It is obvious that (i) the excitons are generated at the EBL interface in the case of NPB:$Ir(piq)_3$ while for the TCTA:$Ir(ppy)_3$ OLED excitons are formed close to the HBL. Using these data, one can deduce the transport character of the EML. Here, NPB:$Ir(piq)_3$ and TCTA:$Ir(ppy)_3$ are preferentially electron and hole transporting, respectively. In the case of the green emitter system, this is in good agreement with data from literature.[9,32] The host NPB is well known as hole transport material which is in contrast to the results presented here.[11,33,34] The electron-transporting character in this OLED structure can be explained by the high emitter concentration of 20 wt %. One can assume that the emitter is present in the host material beyond the percolation limit. Here, the emitter $Ir(piq)_3$ provides good electron transport. This nicely agrees with the results of the triplet-polaron quenching where the best fits were found using the Mott-

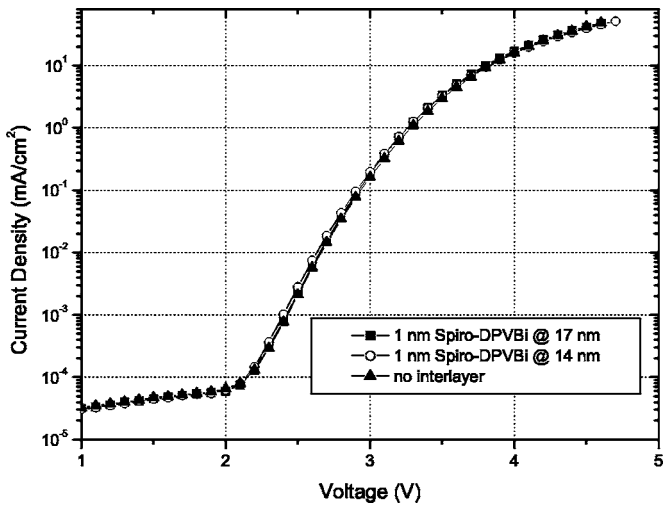

FIG. 11. j-V characteristics of three NPB:$Ir(piq)_3$ OLED's are depicted here. Two OLED's containing sensing layers of 1 nm thickness at different positions are compared with an OLED without such a layer.

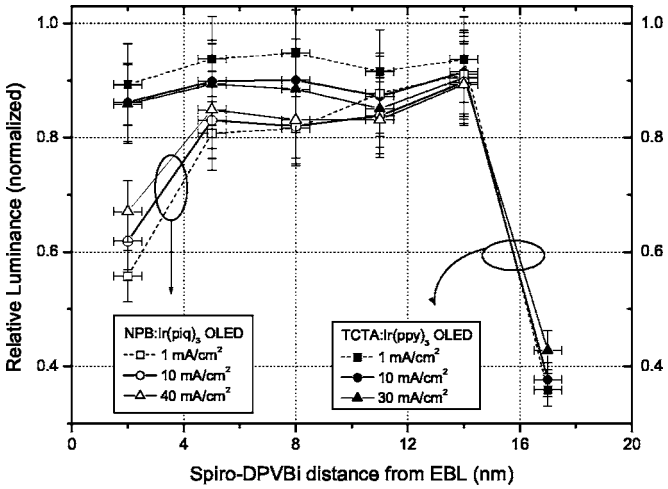

FIG. 12. Intensity of OLED's comprising a sensing layer at different positions relative to a standard OLED. The data points were determined for three different current densities.

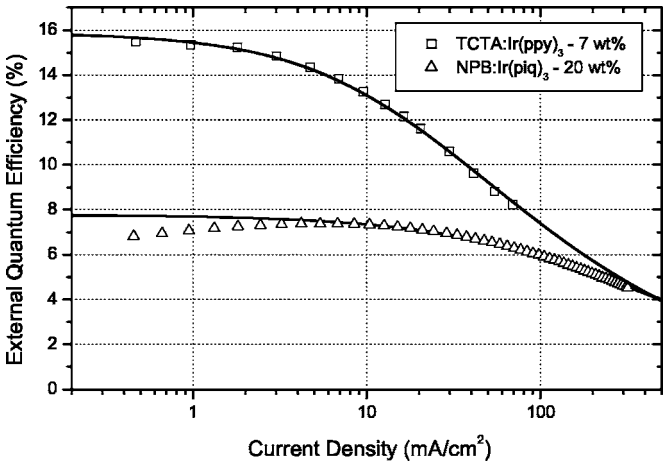

FIG. 13. External quantum efficiency as a function of current density j for both EML systems. Solid lines represent the model calculation according to Eq. (12).

Gurney relation (see Sec. IV B). In this case, the transport is not influenced by charge trap states. (ii) The exciton density profile is broader for the NPB:$Ir(piq)_3$ OLED. This can be appointed to a better charge carrier balance compared to the green OLED. Additionally, a higher diffusion length of the triplet excitons in the red OLED could explain a broader recombination profile. Since the emitter dopant concentration is higher for $Ir(piq)_3$, one could think of an enhanced diffusion probability. (iii) Within experimental error, it can be seen that the exciton formation profile does not change for different current densities j.

V. DISCUSSION

The unified model from Sec. II and the results from Sec. IV yield a consistent picture of the quantum efficiency behavior of phosphorescent OLED's. The external quantum efficiencies of both OLED's introduced here are shown in Fig. 13. Equation (12) from Sec. II is used to model the EQE as a function of current density j. Since this calculation does not include any outcoupling losses, etc., the initial EQE η_0 had to be introduced to scale the fit curves. It will be estimated at low current densities where no quenching is expected. This equation depends on four parameters which can be used to fit the experimental EQE data: τ, k_{TT}, k_P, and w. However, quantitative values could only be determined for the first three. Therefore, experimental values of τ, k_{TT}, and k_P will be implemented into the model calculation without variation, leaving w as the only free fit parameter. Table III summarizes all experimental values used in the calculation. One can see that such OLED's achieve a peak quantum efficiency of 15.8% and 7.6%, respectively. Compared to the NPB:$Ir(piq)_3$ device, the OLED comprising $Ir(ppy)_3$ suffers a stronger roll-off. This is partly due to the higher radiative lifetime for the $Ir(ppy)_3$ system. As previously discussed, the TTA rate constant slightly changes as a function of the initial exciton density $[n_{ex}]$. In the following model calculations, a mean value of this rate constant will be used. The following equation can be used to roughly estimate the exciton density in an OLED under operation conditions:

$$[n_{ex}](j) = \nu \frac{\tau}{ew} j, \tag{18}$$

where ν is the probability of exciton formation. For a typical current density range from 1 mA/cm^2 to 300 mA/cm^2, w = 10 nm, and τ=1.1 μs, the operating OLED's are accompanied by exciton densities from 1×10^{16} cm^{-3} up to 1×10^{18} cm^{-3}. Exactly this range of exciton density is covered by the time-resolved PL experiments. The mean value of the TTA rate constant is therefore calculated in the same exciton density interval as is typical for OLED operation conditions, making this assumption reasonable. In Eq. (12), only the TPQ rate constant of one charge carrier type is used. This is indicated by the bold rate constants in Table III. Here it is assumed that only the majority charge carriers are contributing to the TPQ. This is reasonable since the minority charges will mainly contribute to the exciton formation. In agreement with literature data, the host-guest system TCTA:$Ir(ppy)_3$ of the green OLED is found to be hole transporting.[9,25,32] Therefore, the rate constant $k_{P,h}$ for the hole current is used. The NPB:$Ir(piq)_3$ based OLED is, as discussed in the previous section, preferentially electron transporting in the layer sequence presented here. In this case, the TPQ rate constant for the electron current is used in the calculation.

In Fig. 13, the best fit curves to the OLED EQE of both emitter systems are presented. The curves are in good agreement with the experimental data. For the thickness of the exciton formation zone w, 10 nm and 19 nm are found, where w=10 nm corresponds to the $Ir(ppy)_3$-based OLED. Those values tend to be overestimated because the theory is assuming a constant exciton density profile. This of course is a rough estimation; nevertheless, this parameter can be used to point out differences qualitatively. The calculation suggests that w is about a factor of 2 smaller for the TCTA:$Ir(ppy)_3$ OLED. This difference can also be seen qualitatively in the experiments involving the sensing layer,

TABLE III. Annihilation rate constants and radiative lifetime for both emitter systems. Additionally, the peak EQE is listed. The bold values are used for the model calculation of the specific OLED. In the last column, the thickness of the exciton formation zone is shown which is derived from fit calculations.

	τ [μs]	k_{TT} [10^{-12} cm^3 s^{-1}]	$k_{P,e}$ [10^{-12} cm^3 s^{-1}]	$k_{P,h}$ [10^{-12} cm^3 s^{-1}]	η_0 [%]	w [nm]
TCTA:$Ir(ppy)_3$	(**1.58±0.05**)	(**3±2**)	(0.2±0.1)	(**0.3±0.2**)	**15.8**	10
NPB:$Ir(piq)_3$	(**1.10±0.05**)	(**1.4±0.6**)	(**0.7±0.2**)	(0.2±0.2)	**7.6**	19

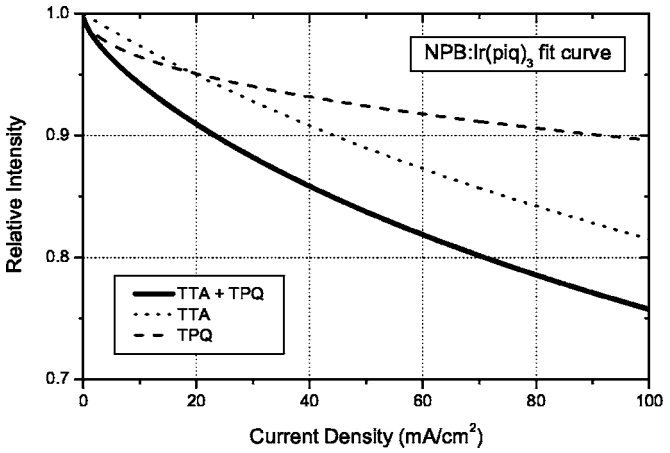

FIG. 14. Solid line: model calculation of the NPB:$Ir(piq)_3$ based OLED. The other two curves are generated by ignoring one or the other quenching process. The plot is on linear scale for better visibility.

as shown previously. Here, a smaller value of w enhances triplet quenching since the exciton density increases in order to achieve the same brightness. In addition, the longer triplet lifetime τ and the slightly higher TTA rate constant k_{TT} of the TCTA:$Ir(ppy)_3$ system explain the stronger efficiency roll-off observed for the green OLED. On the other hand, the red NPB:$Ir(piq)_3$ shows advances in all parameters, having a shorter lifetime τ, smaller k_{TT}, and a broader exciton formation zone w (cf. Table III). For this OLED, a rather moderate efficiency decrease can be observed (see Fig. 13). Nevertheless, the absolute efficiency of the green TCTA:$Ir(ppy)_3$ is higher which is due to a higher internal PL efficiency.[35] Baldo *et al.* reported in their study that they could not fit the EQE of an OLED comprising CBP doped with $Ir(ppy)_3$ with a single value of k_{TT}.[12] Instead, they used two different values for k_{TT} to find good agreement with the experimental data. They explained this behavior by interactions between CBP and $Ir(ppy)_3$. Even if the devices presented here differ in the host material—i.e., TCTA—one can see that the calculated fit according to the unified model nicely agrees with the EQE data.

The fit calculation of the NPB:$Ir(piq)_3$ OLED can now be used to show the magnitude of TTA and TPQ individually. Consecutively, one of the two rate constants k_{TT} and k_P is set to zero. The result is shown in Fig. 14. One can see that the contribution of TTA is stronger than TPQ going to high current densities. This is reasonable because the exciton density $[n_{ex}]$ in Eq. (11) appears quadratically for TTA while only linearly for TPQ. Nevertheless, at low current densities the EQE is mainly reduced by triplet-polaron quenching. It can be seen that both quenching processes contribute to the efficiency roll-off in the OLED's presented here. This becomes

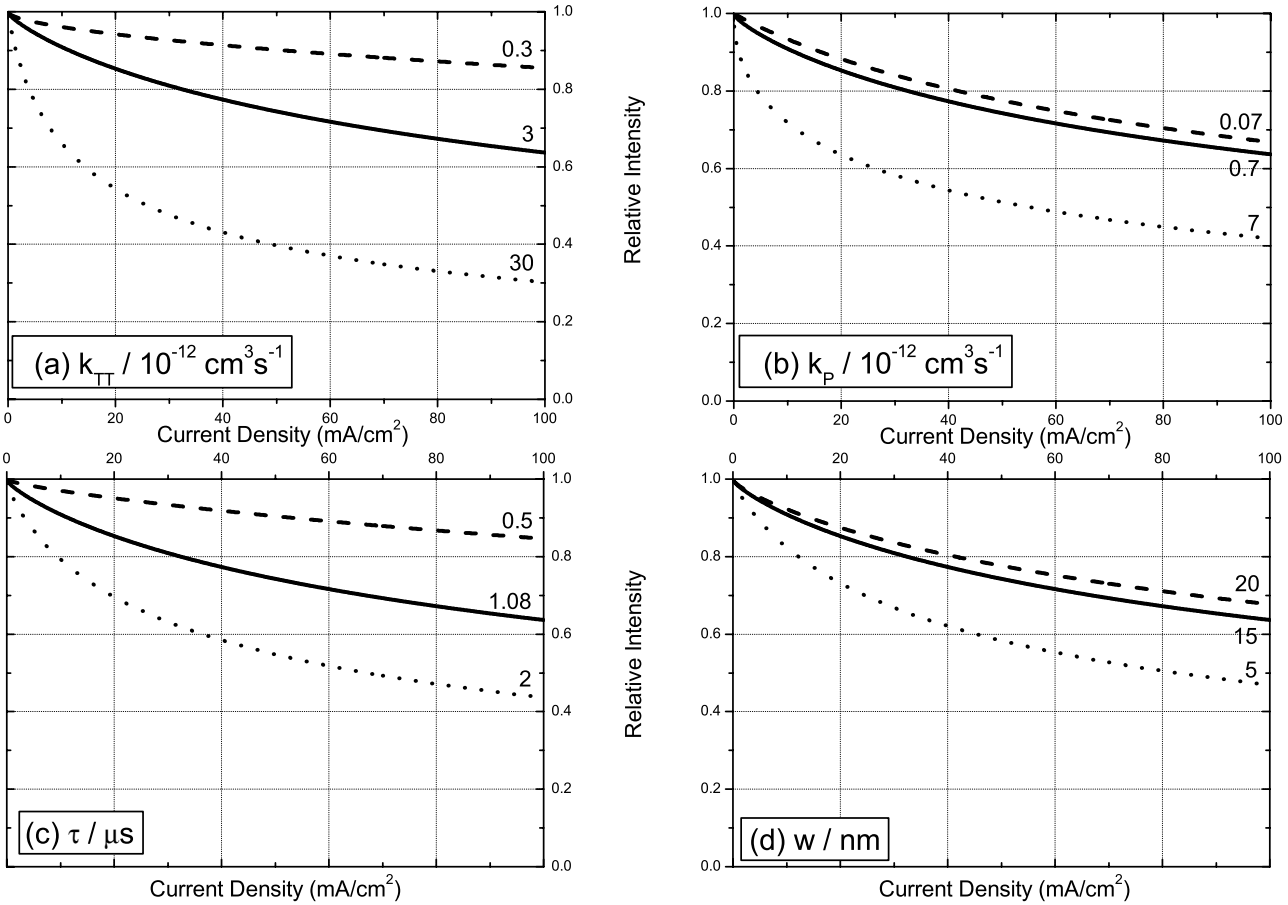

FIG. 15. Variation of parameters (a) k_{TT}, (b) k_P, (c) τ, and (d) w using the model calculation. Solid line: fit calculation of the NPB:$Ir(piq)_3$ device (see Fig. 13). Values used for the various parameters are depicted in the plot.

different when the triplet lifetime τ of the emitter molecule is much larger—e.g., for PtOEP with $\tau \sim 110\ \mu s$ in a CBP matrix.[12] In this case, the probability of TTA is enhanced resulting in a triplet-triplet dominated roll-off as reported by Baldo *et al.*[11,12] and Canzler and Kido.[36]

Using the model calculation, the influence of quenching rate constants, radiative lifetime, and exciton formation zone on the OLED performance can be shown. Therefore, the fit curve of the NPB:$Ir(piq)_3$ device with its corresponding parameters is plotted in Fig. 15 as the solid line. Taken this as basis, all parameters are varied consecutively in plots (a)–(d). It can be seen that all parameters influence the OLED efficiency in a certain manner. For example, the phosphorescent lifetime τ [Fig. 15(c)] strongly affects the device performance. Here, the value of τ is only varied by a factor of 4. Nevertheless, it remains doubtful if they can be tuned so that the efficiency roll-off can be decreased. For example, both the triplet-triplet annihilation rate constant k_{TT} and the radiative lifetime τ seem to be inaccessible. The triplet lifetime, of course, can be tuned by materials science, but the phosphorescent emitters used here are already optimized for short lifetimes. The parameters k_P and w can be brought into the optimum by optimizing the OLED architecture, resulting in a broad exciton distribution within the EML without any charge accumulation. This has been demonstrated sucessfully by the double-emission layer approach.[9,32] There, two matrices with different transport properties are combined to achieve a broad emission zone centered in the center of the EML.

VI. CONCLUSIONS

In this study, it could be shown that both triplet-triplet annihilation and triplet-polaron quenching influence the efficiency roll-off in state-of-the-art phosphorescent OLED's. In our study, OLED's comprising TCTA:$Ir(ppy)_3$ and NPB:$Ir(piq)_3$, respectively, are used as example devices. Both TTA and TPQ are investigated quantitively, expressed by rate constants k_{TT} and k_P. A unified model is introduced, taking both processes into account. By implementing the experimentally determined rate constants in such a calculation, good agreement with the η_{ext}-j characteristics is found. As a next step, this model is used to discuss the different magnitudes of the above-mentioned processes under OLED operation conditions. The calculation showed further that approaches to decrease the efficiency roll-off are rather limited. In the systems we studied, many parameters influencing the EQE seem to be close to the optimum already. Finally, field-induced quenching could be excluded as a relevant process in such devices.

ACKNOWLEDGMENTS

This work was funded by the European Commission within the sixth framework IST program under Contract No. IST-2002-004607, project "OLLA," and via the Leibniz prize of the Deutsche Forschungsgemeinschaft.

*Electronic address: karl.leo@iapp.de; URL: http://www.iapp.de

[1] C. W. Tang and S. A. Van Slyke, Appl. Phys. Lett. **51**, 913 (1987).
[2] C. W. Tang, S. A. Van Slyke, and C. H. Chen, J. Appl. Phys. **65**, 3610 (1989).
[3] M. A. Baldo, D. F. O'Brien, Y. You, A. Shoustikov, S. Sibley, M. E. Thompson, and S. R. Forrest, Nature (London) **395**, 151 (1998).
[4] C. Adachi, M. A. Baldo, S. R. Forrest, and M. E. Thompson, Appl. Phys. Lett. **77**, 904 (2000).
[5] C. Adachi, M. A. Baldo, M. E. Thompson, and S. R. Forrest, J. Appl. Phys. **90**, 5048 (2001).
[6] N. Greenham, R. Friend, and D. Bradley, Adv. Mater. (Weinheim, Ger.) **6**, 491 (1994).
[7] M. Pfeiffer, K. Leo, X. Zhou, J. S. Huang, M. Hofmann, A. Werner, and J. Blochwitz-Nimoth, Org. Electron. **4**, 89 (2003).
[8] X. Zhou, J. Blochwitz, M. Pfeiffer, A. Nollau, T. Fritz, and K. Leo, Adv. Funct. Mater. **11**, 310 (2001).
[9] G. He, M. Pfeiffer, K. Leo, M. Hofmann, J. Birnstock, R. Pudzich, and J. Salbeck, Appl. Phys. Lett. **85**, 3911 (2004).
[10] M. Pope and C. E. Swenberg, *Electronic Processes in Organic Crystals* (Oxford University Press, New York, 1999).
[11] M. A. Baldo and S. R. Forrest, Phys. Rev. B **62**, 10958 (2000).
[12] M. A. Baldo, C. Adachi, and S. R. Forrest, Phys. Rev. B **62**, 10967 (2000).
[13] W. Stampor, J. Kalinowski, P. Di Marco, and V. Fattori, Appl. Phys. Lett. **70**, 1935 (1997).
[14] J. Kalinowski, W. Stampor, J. Mezyk, M. Cocchi, D. Virgili, V. Fattori, and P. Di Marco, Phys. Rev. B **66**, 235321 (2002).
[15] J. Mezyk, J. Kalinowski, F. Meinardi, and R. Tubino, Appl. Phys. Lett. **86**, 111916 (2005).
[16] R. G. Kepler, J. C. Caris, P. Avakian, and E. Abramson, Phys. Rev. Lett. **10**, 400 (1963).
[17] T. Tsuboi, J. Lumin. **119-120**, 288 (2006).
[18] T. Förster, Ann. Phys. **2**, 55 (1948).
[19] J. Simon and J.-J. Andre, *Molecular Semiconductors* (Springer-Verlag, Berlin, 1985).
[20] D. L. Dexter, J. Chem. Phys. **21**, 836 (1953).
[21] V. Ern, H. Bouchriha, J. Fourny, and G. Delacote, Solid State Commun. **9**, 1201 (1971).
[22] S. Berleb, Ph.D. thesis, Universität Bayreuth, 2001.
[23] M. A. Lampert, Rep. Prog. Phys. **27**, 329 (1964).
[24] P. W. M. Blom, C. Tanase, D. M. de Leeuw, and R. Coehoorn, Appl. Phys. Lett. **86**, 092105 (2005).
[25] G. He, O. Schneider, D. Qin, X. Zhou, M. Pfeiffer, and K. Leo, J. Appl. Phys. **95**, 5773 (2004).
[26] J. Lam, T. Gorjanc, Y. Tao, and M. D'Iorio, J. Vac. Sci. Technol. A **18**, 593 (2000).
[27] J. Kalinowski, J. Mezyk, F. Meinardi, R. Tubino, M. Cocchi, and D. Virgili, J. Appl. Phys. **98**, 063532 (2005).
[28] W. Holzer, A. Penzkofer, and T. Tsuboi, Chem. Phys. **308**, 93 (2005).

[29] R. Krause, Master's thesis, Technische Universität Dresden, 2005.
[30] M. A. Baldo and S. R. Forrest, Phys. Rev. B **64**, 085201 (2001).
[31] M. I. Khan, G. C. Bazan, and Z. D. Popovic, Chem. Phys. Lett. **298**, 309 (1998).
[32] X. Zhou, D. S. Qin, M. Pfeiffer, J. Blochwitz-Nimoth, A. Werner, J. Drechsel, B. Männig, K. Leo, M. Bold, and P. Erk, Appl. Phys. Lett. **81**, 4070 (2002).
[33] M. A. Baldo, M. E. Thompson, and S. R. Forrest, Pure Appl. Chem. **71**, 2095 (1999).
[34] J. Feng, F. Li, W. Gao, S. Liu, Y. Liu, and Y. Wang, Appl. Phys. Lett. **78**, 3947 (2001).
[35] A. Tsuboyama, H. Iwawaki, M. Furugori, T. Mukaide, J. Kamatani, S. Igawa, T. Moriyama, S. Miura, T. Takiguchi, and S. Okada, J. Am. Chem. Soc. **125**, 12971 (2003).
[36] T W. Canzler and J. Kido, Org. Electron. **7**, 29 (2006).